DETERMINATION AND IDENTIFICATION OF ATOMIC STRUCTURE OF AMORPHOUS ALLOYS

Supplement to Sci. Rep. RITU, A, June, 1978

DETERMINATION AND IDENTIFICATION OF ATOMIC STRUCTURE OF AMORPHOUS ALLOYS

Toru Imura, Minoru Doi and Hitoshi Kosaki

Department of Metallurgy, Faculty of Engineering,

Nagoya University, Furo-cho, Chikusa-ku, Nagoya 464, Japan

ABSTRACT

High resolution electron microscopy (interference image microscopy), field-ion microscopy and high voltage electron microscopy were successfully used in combination with X-ray and/or electron diffraction method to investigate the structure and the thermal stability of liquid-quenched Fe-P, Fe-P-C, Fe-B-Si and Ni-B-Si alloys in conjunction with quenching methods and preparation conditions.

The untilted interference images and field-ion images of the liquid-quenched alloys prepared by drum-quenching method and by roller-quenching method at a fast quenching rate yielded no evidence of the existence of microcrystallites larger than several atomic spacings in diameter. However, a periodical fringe-like contrast indicating the existence of a regular atomic arrangement was locally observed in the alloys quenched at slower quenching rate. A periodical fringe-like contrast was also observed in the regions adjacent to the crystalline phase in the amorphous alloys partially crystallized by heating. Furthermore, a circular arrangement of image spots indicating the existence of a regular atomic arrangement was also observed locally in the field-ion image of the tipped specimen heated at a temperature below the crystallization temperature. These regions, in which the periodical fringe-like contrast or the circular arrangement of image spots were observed, yielded only halo rings in their diffraction patterns. Therefore, to characterize amorphous alloys prepared by various methods under different conditions or to identify those amorphous alloys, the directer methods such as high resolution electron microscopy and/or field-ion microscopy must be used in combination with X-ray or electron diffraction method which has been usually used in most cases so far.

When thin foil specimens of liquid-quenched Fe-P, Fe-P-C and Ni-B-Si amorphous alloys were heated in-situ under the irradiation of 400keV elec-

trons in a high voltage electron microscope, two types of electron irradiation effect were observed; one is an acceleration of crystallization, which was observed in the Ni-B-Si amorphous alloy, and the other is a retardation of crystallization, which was observed in the Fe-P and Fe-P-C amorphous alloys.

Pole figure determinations suggest that no preferred orientation was developed appreciably in the crystallization processes of the liquid-quenched Fe-P-C amorphous alloy and also the cold-rolled sheet of this alloy.

In the case of room temperature deformation, the load-elongation curves of the Fe-P-C and Fe-B-Si alloys prepared at the faster quenching rate indicate some deviation from the linearity well below the fracture point. While in the case of the alloys which were prepared at the slower quenching rate and which exhibited a periodical fringe-like contrast in the untilted interference images, the load-elongation curves were almost straight and practically no deviation was observed up to fracture. Scanning electron microscope observations of the fractured surfaces revealed that the shear displacement occurred in the alloys prepared at the faster quenching rate but not in the alloys prepared at the slower quenching rate. After a series of loading-unloading stress cycles where the maximum load of each stressing cycle was gradually increased, the load-elongation curves of the Fe-P-C and Fe-B-Si alloys prepared at the faster quenching rate became straighter and the deviation from the linearity was much smaller even at the fracture point.

INTRODUCTION

Duwez and his colleagues reported for the first time in 1960 that rapid quenching from the melt (so-called liquid-quenching) of an eutectic alloy gave a new metastable phase of non-crystalline structure [1]. The eutectic alloy studied by them at that time was 25 atomic percent silicon-gold binary alloy but nowadays, besides a few hundred of binary alloys, a number of ternary and more complex alloys are known to be rapidly quenched from the melt by means of various liquid-quenching methods without forming crystalline phase [2,3]. These alloys are called amorphous alloys or glassy metals or sometimes metallic alloy glasses, etc.

Amorphous alloys in general do not show any definite contrast in the bright-field images obtained by conventional transmission electron microscopy but yield only diffuse halo rings in their diffraction patterns. Therefore, several kinds of structure model, which interpret halo rings in diffraction pattern, have been proposed; for instance, "microcrystalline model", "dense random packing model", "random layer model", etc. [4,5].

As well known, amorphous alloys investigated so far exhibit some interesting physical, chemical and mechanical properties which are different from those of the ordinary crystalline materials. Furthermore, there are still some possibilities that materials which have unforeseen properties may be found from among amorphous alloys. The properties characteristic of amorphous alloys are, of course, attributable to their atomic arrangements. Therefore, atomic structure of amorphous alloys have to be fully investigated at first in conjunction with quenching method and preparation conditions.

By the way, it is questionable that so-called liquid-quenched amorphous alloys prepared by various methods under different conditions have a common definite atomic structure. Ideal amorphous alloys may have a definite structure which is interpreted by one of the models proposed so far, such as, dense random packing model. In the case of actual amorphous alloys prepared, however, there is a possibility that atomic arrangement would be different more or less, depending on the methods and conditions of preparation.

Most of the structure studies which have been made so far are based on the analysis of diffraction patterns, namely, the radial distribution analysis of diffraction halos [4,5]. But it is hard to believe that the radial distribution analysis yields one discrete structure model without ambiguity, because it provides indirect information about atomic configuration averaged over a large area. Consequently, the directer method such as high resolution electron microscopy etc. must be used in combination with the indirect method to detect or to identify the local fluctuations of the amorphous structure.

In the present studies, structure-determination methods such as high resolution electron microscopy, field-ion microscopy and high voltage electron microscopy were successfully used in combination with X-ray or electron diffraction method to investigate the structure and the thermal stability of liquid-quenched Fe-based and Ni-based amorphous alloys prepared by using either the drum-quenching method or the roller-quenching method under varying conditions. Mechanical properties of Fe-based amorphous alloys were also studied, being related to the condition of preparation.

PREPARATION METHOD USED FOR LIQUID-QUENCHING

Drum-quenching method and roller-quenching method were used for liquid-quenching of $Fe_{80}P_{13}C_7$, $Fe_{78}P_{15}C_7$, $Fe_{78}B_{12}Si_{10}$ and $Ni_{75}B_{17}Si_8$ alloys. The thin ribbon specimens of about 20~40 μm thick were prepared. The rotation speed of the drum of 130 mmϕ with copper lining was about 6000 r.p.m. and that of the twin rollers of 50 mmϕ made of carbon tool steel was varied in the range of 2700 r.p.m. to 5400 r.p.m., although at the rotation speed of 4500 r.p.m. the maximum quenching rate was achieved. The fast quenching rate described hereafter means the rotation speed of the range 4050 r.p.m. to 4950 r.p.m. and the slower quenching rate means that of the range below 4000 r.p.m. or above 5000 r.p.m.

STRUCTURE-DETERMINATION METHODS

In table 1, various methods for determining structure of amorphous alloys are summarized. Among these, X-ray or electron diffraction analysis has been generally used to determine and to identify the atomic structure. In this case, coordination number, the nearest neighbor distance, number and distance of the second neighbor, etc. are calculated from the radial distribution function which is obtained from the angular dependence of scattered intensity measured.

Figures 1(a) and (b) are schematic diagrams illustrating the geometry

Table 1. Structure-determination methods of amorphous alloys

*ELECTRON, X-RAY OR NEUTRON DIFFRACTION METHOD (RADIAL DISTRIBUTION ANALYSIS)
Coordination Number, Nearest Neighbor Distance, etc.

*HIGH RESOLUTION ELECTRON MICROSCOPY
Interference Image (Lattice Image).
Dark-Field Image.

*FIELD-ION MICROSCOPY
Direct Observation of the Atomic Structure of Solid Surface in Atomic Scale.

for so-called direct-resolution microscopy (i.e., interference image microscopy or lattice-imaging as it is often called) using tilted illumination or untilted illumination. In the case of the tilted illumination, incident electron beam is tilted so that the optical axis of microscope is placed just halfway between the direction of transmitted beam and that of diffracted beam which forms the first halo ring. The transmitted beam and a part of the diffracted beam can pass through the objective aperture [6]. This method is called the tilted illumination interference microscopy. While in the case of the untilted illumination, the incident beam is not tilted and both the transmitted beam and the diffracted beam which forms the first halo ring can pass through the objective aperture. This method is called the

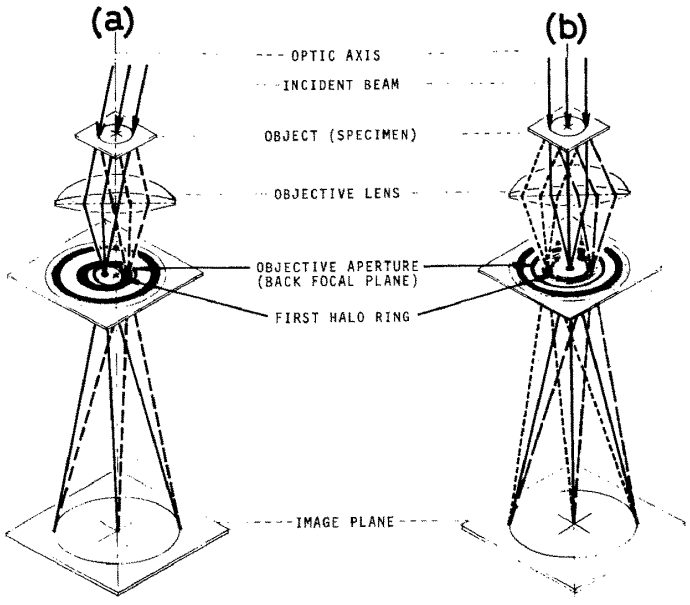

Figure 1. Schematic diagrams illustrating the geometry for so-called direct-resolution microscopy; tilted illumination interference microscopy (a), and untilted interference image microscopy (b).

untilted interference image microscopy [7]. If the periodic arrangements of atoms (i.e., crystalline phase) is present in a foil specimen, the diffracted beam which carries the information on the periodicity may be recombined with the transmitted beam to yield the direct-resolution phase-contrast image under an appropriate condition, so that we may expect to observe lattice fringes.

By means of field-ion microscopy, the atomic structure of solid surface can directly observed because of its high magnification and resolution. The direct observation like this is unique and not easy to be achieved by other methods such as the conventional electron microscopy. But this field-ion microscope observation has a serious restriction in relation to the fact that the surface of a tiny tipped specimen whose radius is at most some thousand Å can be observed under a very high electric field.

HIGH RESOLUTION ELECTRON MICROSCOPY

For high resolution electron microscope observation, thin foil specimens were prepared by electropolishing the as liquid-quenched ribbon specimens or the annealed ones. The untilted inteference image microscopy was used in the present studies because the tilted beam tends to introduce astigmatism in an otherwise essentially astigmatic-free beam and this leads to the directional filtering [7].

Figures 2 and 3 illustrate the high resolution electron micrograph of as drum-quenched $Fe_{84}P_{16}$ alloy and that of as roller-quenched $Fe_{78}P_{15}C_7$ alloy, respectively. In most of the through focal series of the liquid-quenched alloys examined so far, the regular lattice fringe suggesting the existence of microcrystallites larger than several atomic spacings has not been recognized. However, in the untilted interference images of the liquid-quenched alloys prepared at slower quenching rate, a periodical fringe-like contrast was observed locally as illustrated in Fig. 4, although the diffraction patterns of the alloys consisted of only ordinary halo rings. This fringe-like contrast is maybe resulted from the existence of a periodical atomic arrangement, that is, a sort of microcrystallites.

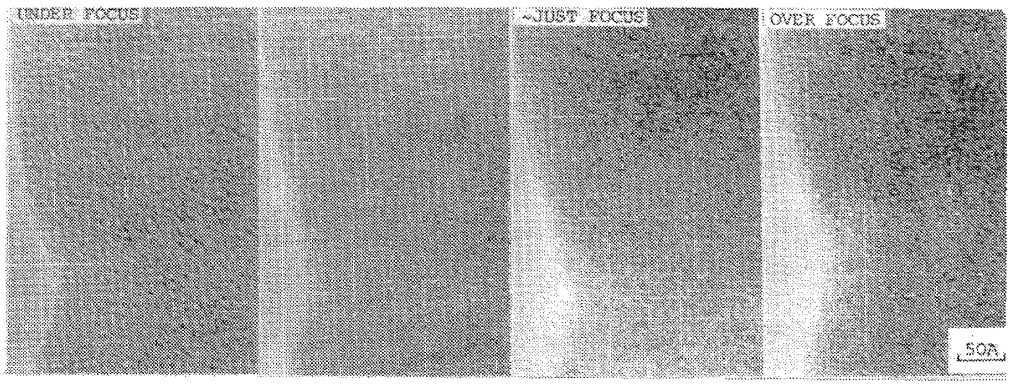

Figure 2. Untilted interference images of as drum-quenched $Fe_{84}P_{16}$ alloy showing a blob-like contrast.

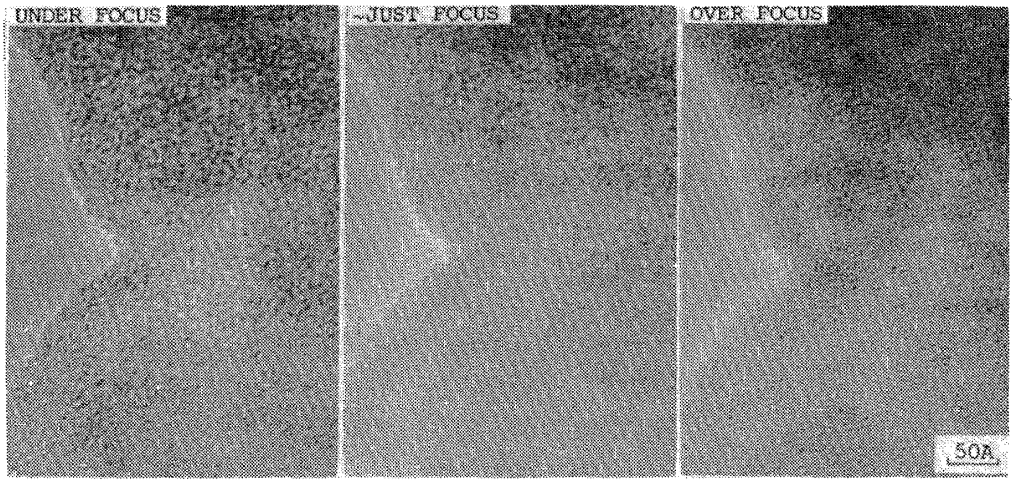

Figure 3. Untilted interference images of as roller-quenched $Fe_{78}P_{15}C_7$ alloy showing a blob-like contrast.

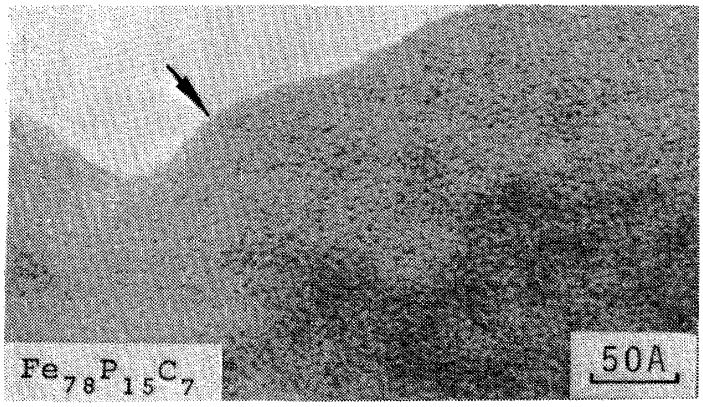

Figure 4. Untilted interference image of as roller-quenched $Fe_{78}P_{15}C_7$ alloy prepared at the slower quenching rate, showing a fringe-like contrast locally.

Figure 5 illustrates the untilted interference image of partially crystallized $Fe_{78}P_{15}C_7$ alloy. A periodical fringe-like contrast was also observed in the area which was adjacent to crystalline phase, although the diffraction pattern of this area consisted of only halo rings. This contrast may be regarded as the evidence of the existence of small domains which exhibit the periodical atomic arrangements with some regularity. Therefore, it seems that a crystal-like zone exists around the crystalline phase in the amorphous alloy partially crystallized by heating, and the regularity of atomic arrangement in this transitional zone may be intermediate between the amorphous phase and the crystalline phase.

FIELD-ION MICROSCOPY

Tipped specimens for field-ion microscope (FIM) observations were pre-

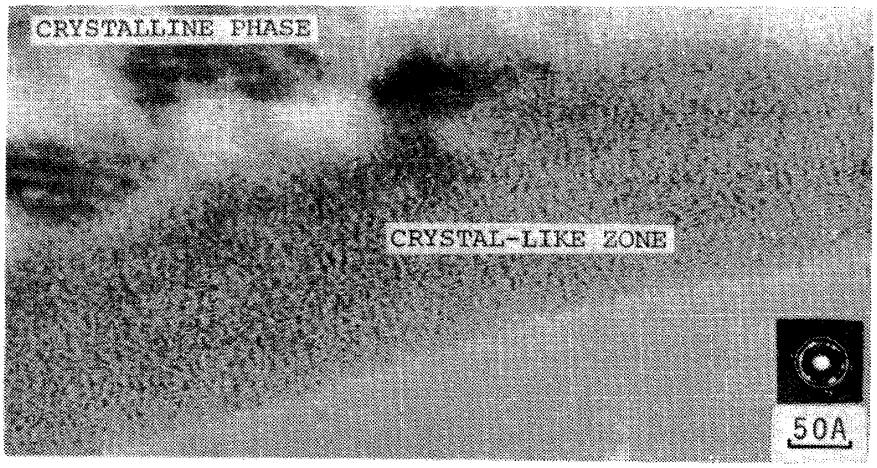

Figure 5. Untilted interference image of partially crystallized $Fe_{78}P_{15}C_7$ amorphous alloy showing crystal-like zone around crystalline phase.

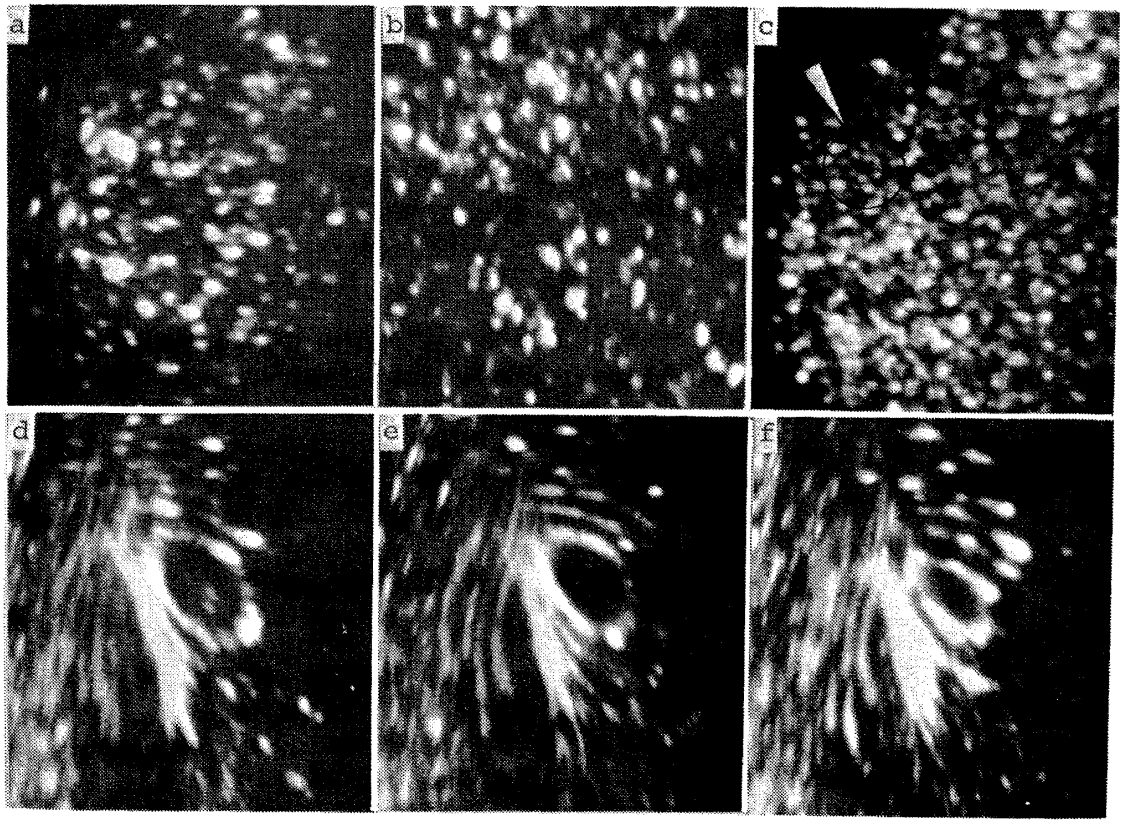

Figure 6. Field-ion images of liquid-quenched $Fe_{80}P_{13}C_7$ alloy; (a,b) liquid-quenched, (c) annealed at 430°C below the crystallization temperature for 10 min, indicating a circular arrangement of image spots, (d,e,f) crystallized at 620°C, indicating the changes of ring pattern due to successive applications of field evaporation.

pared by electropolishing the liquid-quenched alloys and all the FIM observations in the present experiment were made at liquid nitrogen temperature by using a mixture of helium and hydrogen (about 1 % by volume) as an imaging gas.

Figures 6(a) and (b) illustrate FIM images of liquid-quenched $Fe_{80}P_{13}C_7$ alloys. These images are far different from the clear ring patterns which appeared in the crystallized specimen, and which are shown in Figs. 6(d), (e) and (f). By the FIM observations of the as liquid-quenched alloys, decisive evidence of the existence of microcrystallites or crystalline clusters larger than several atomic spacings has not been obtained so far. This observation is supported by the untilted interference image microscopy of the liquid-quenched alloys mentioned before.

Figure 6(c) illustrates a FIM image of the $Fe_{80}P_{13}C_7$ alloy which was liquid-quenched and heated in-situ at 430°C for 10 min in a FIM. When a foil specimen of the liquid-quenched $Fe_{80}P_{13}C_7$ amorphous alloy was heated in-situ at the rate of less than 2°C/min in a high voltage electron microscope, a crystalline phase did not appear until the heating temperature was raised above 450°C. However, some changes were recognized in the FIM image of the tip heated at a temperature even below the crystallization temperature at which the nucleation of crystalline phase was clearly observed in the case of the conventional electron microscope observation. Namely, the circular arrangement of image spots was sometimes observed in the FIM image of the tip heated in-situ at 430°C in a FIM, as marked by the circle in Fig. 6(c), although the electron diffraction pattern of the tip consisted of only halo rings. This circular arrangement of image spots indicates that a crystalline cluster, which has a possibility of being a nuclei of crystalline phase, may exist in the region.

ELECTRON DIFFRACTION AND HIGH VOLTAGE ELECTRON MICROSCOPY

Figure 7(a) illustrates a microphotometer trace of the transmission electron diffraction pattern of the as liquid-quenched $Fe_{80}P_{13}C_7$ alloy. This profile was not appreciably changed by the irradiation of 100~1000 keV electrons up to the total dose of about 10^{23} electrons/cm^2 at room temperature.

However, the thin foil specimen was heated in-situ up to 200°C in a high voltage electron microscope (HVEM), the splitting of the second halo ring disappeared by the irradiation of 400 keV electrons of the total dose of about 2×10^{22} electrons/cm^2, while no appreciable change occurred in the unirradiated region of the same specimen, as shown in Figs. 7(b) and (c).

As the temperature was raised at the rate of about 2°C/min, nucleation of crystalline phase started at 450°C. At 490°C, nucleation and growth of crystalline phase were observed in most part of the specimen. However, in the thinner part of the foil specimen or in the area which was irradiated by high dose of 400 keV electrons, crystalline phase did not appear up to more than 500°C (cf. Fig. 8).

The similar phenomena were also observed in the liquid-quenched $Fe_{84}P_{16}$

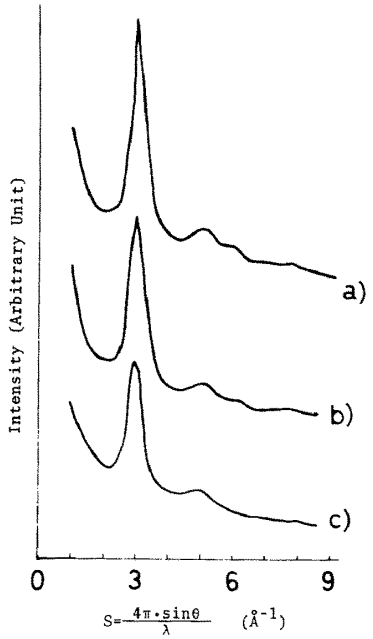

Figure 7. Microphotometer traces of the electron diffraction patterns of $Fe_{80}P_{13}C_7$ amorphous alloy; liquid-quenched (a), annealed at 200°C (b), and irradiated by focused 400 keV electrons at 200°C (c).

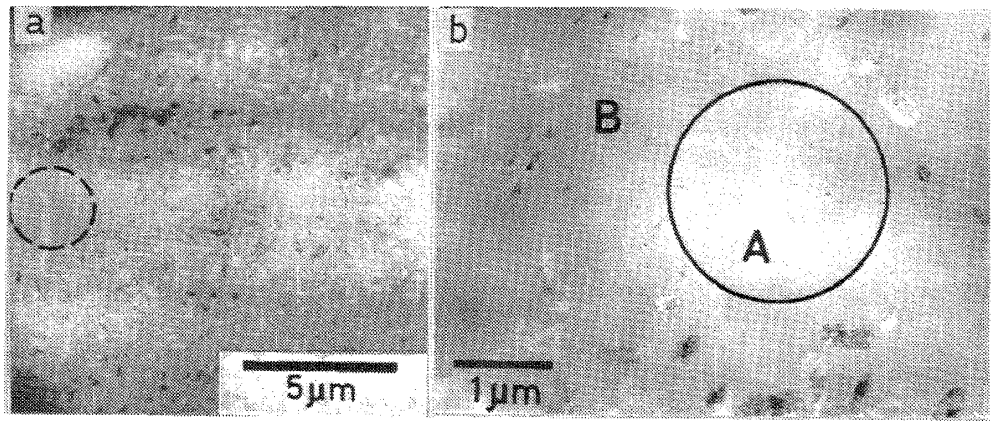

Figure 8. Transmission electron micrographs indicating the crystallization stage of $Fe_{80}P_{13}C_7$ amorphous alloy; in the thinner part (inside the circle) (a), and in the area irradiated intentionally by high dose of 400 keV electrons (inside the circle A) (b).

amorphous alloy. When in-situ heating was made in the same manner as the case of the $Fe_{80}P_{13}C_7$ amorphous alloys, the entire specimen except for the irradiated region was covered by a crystalline phase at 240°C, as shown in Fig. 9. But crystallization did not occur in the irradiated region up to about 320°C. In these cases, the electron irradiation effect is an retardation of crystallization, namely, the improvement of thermal stability.

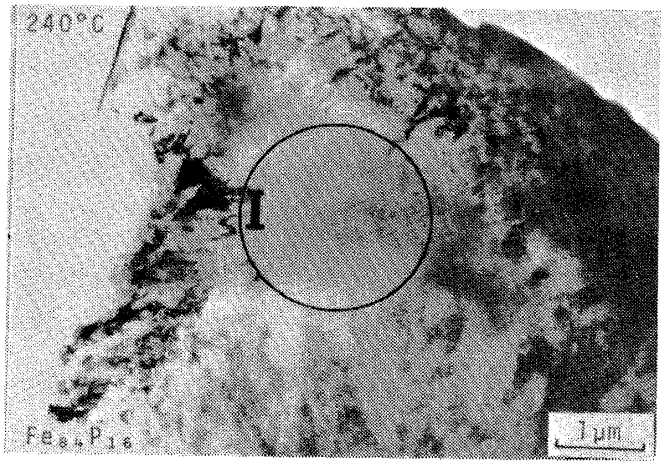

Figure 9. Transmission electron micrograph indicating the retardation of crystallization in the electron (400 keV) irradated region marked by the circle I.

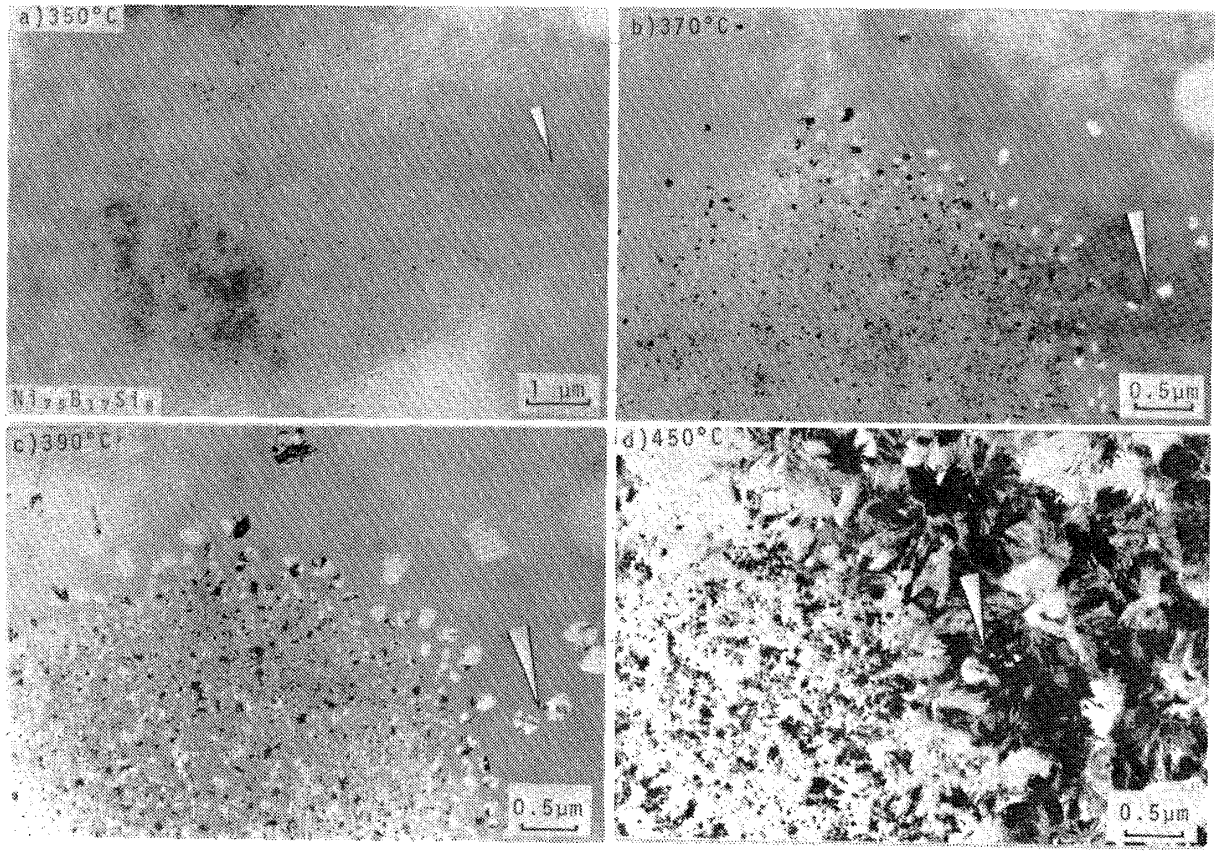

Figure 10. Transmission electron micrographs indicating the crystallization stages of $Ni_{75}B_{17}Si_8$ amorphous alloy. An arrow marked on each micrograph indicates the same location on the specimen surface. Crystallization was accelerated by the irradiation of 400 keV electrons.

Figure 10 illustrates the crystallization process of the liquid-quenched $Ni_{75}B_{17}Si_8$ amorphous alloy. In-situ heating of this amorphous alloy was made at the rate of 5°C/min under the irradiation of 400 keV electrons at the dose rate of 2.4×10^{18} electrons$\cdot cm^{-2} \cdot sec^{-1}$ in a HVEM. When the heating temperature was raised up to about 330°C, a crystalline phase appeared at first in the region which was intentionally irradiated by focused 400 keV electrons. At 350°C, nucleation and growth of the crystalline phase were observed only in the irradiated region, as shown in Fig. 1o(a). In the unirradiated region, however, the crystallization did not occur until the heating temperature was raised up to about 370°C, as indicated by an arrow in Fig. 10(b). These crystalline grains in both regions have the face-centered cubic structure and are considered to be the metastable phase I (so-called MS-I phase) which was reported by Masumoto and others [8], judging from the diffraction pattern and the appearence of the crystalline grains. Furthermore, the crystalline grains in the irradiated region are numerous and much finer than those in the unirradiated region, as shown in Fig. 10(c). In this case, the electron irradiation effect is an acceleration of crystallization, namely, the lowering of thermal stability.

With increasing the temperature, a new crystalline phase appeared at about 450°C in uncrystallized amorphous matrix and the entire specimen was covered by two types of crystalline phase, as shown in Fig. 10(d). This new crystalline phase is considered to be the metastable phase II (so-called MS-II phase) which was also reported by Masumoto and others [8]. A lattice fringe electron micrograph of the MS-II phase is illustrated in Fig. 11.

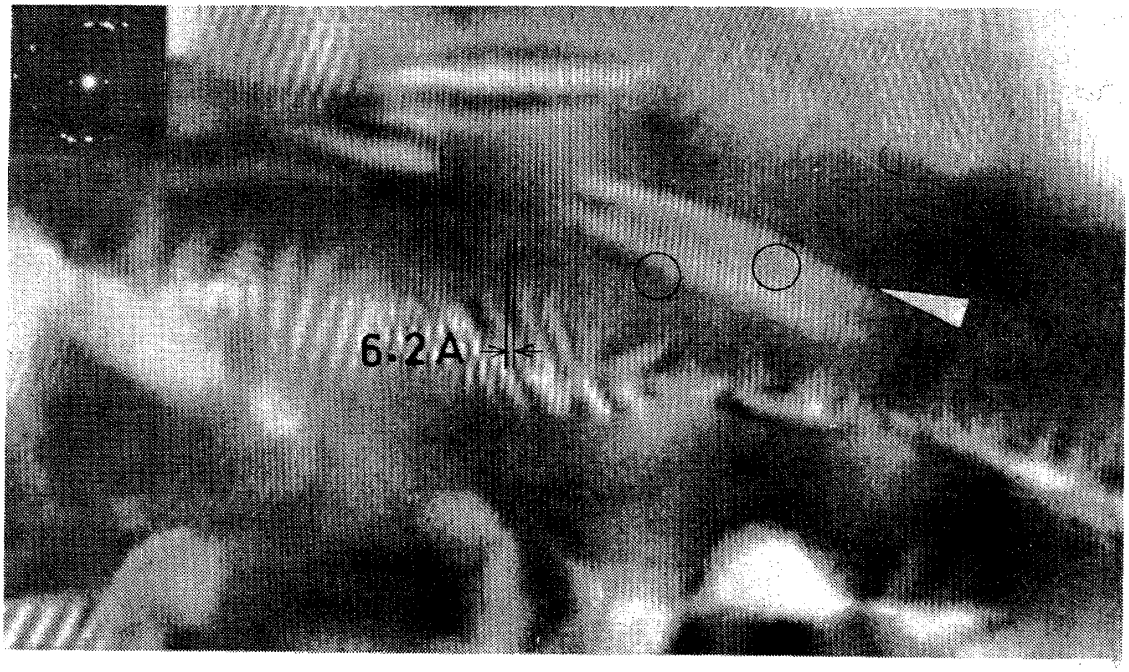

Figure 11. Lattice-imaging of the crystalline metastable phase (so-called MS-II phase) in crystallized $Ni_{75}B_{17}Si_8$ amorphous alloy. An arrow indicates a subgrain boundary and dislocations are observed as marked by the two circles.

The lattice fringe of 6.2 Å spacing can be seen in this micrograph. The lattice imaging suggest that the MS-II phase consists of small subgrains, one of which is indicated by the arrow in the micrograph. Dislocations are also observed as marked by the circles.

In the present experiment, two types of electron irradiation effect were observed; one was an acceleration of crystallization which was observed in the Ni-B-Si amorphous alloy and the other was a retardation of crystallization which was observed in the Fe-P and Fe-P-C amorphous alloys. The reason why some amorphous alloys exhibited the retardation and some the acceleration is not clear at the moment. More systematic observations are needed to explain the phenomena.

X-RAY DIFFRACTION ANALYSIS

The pole figure which was obtained by using the reflection which produces the first halo ring of the as liquid-quenched $Fe_{80}P_{13}C_7$ alloy pre-

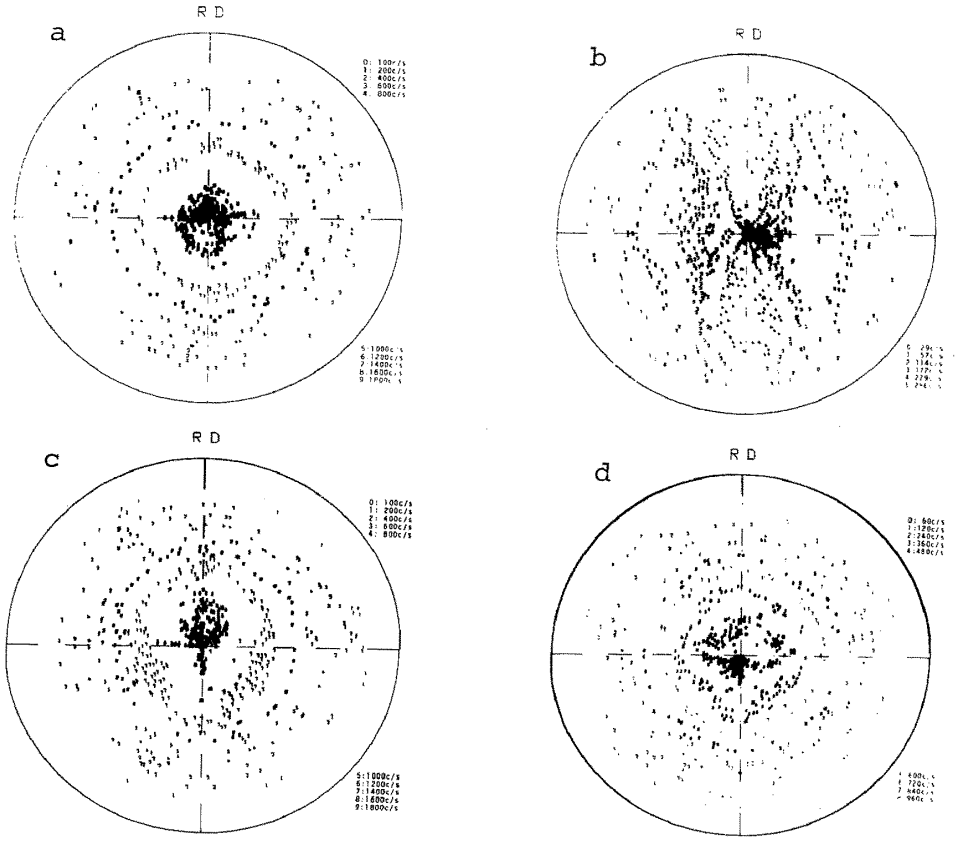

Figure 12. Pole figures obtained with liquid-quenched $Fe_{80}P_{13}C_7$ alloy; (a) as liquid-quenched (taken with the first halo ring), (b) heated at 600°C after the liquid-quenching (taken with the (200) reflection of αFe matrix), (c) cold-rolled after the liquid-quenching (taken with the first halo ring), and (d) heated at 600°C after cold-rolling of the liquid-quenched alloy (taken with the (110) reflection of αFe matrix).

ared at a fast quenching rate is illustrated in Fig. 12(a). The pole figure obtained with the (200) reflection of αFe matrix in the $Fe_{80}P_{13}C_7$ alloy which was crystallized at 600°C is also illustrated in Fig. 12(b). The direction denoted by "RD" in Fig. 12 corresponds to the direction of solidification. Each of these figures looks as if the preferred orientations were present in those specimens. However, taking into account of areal contraction at the center of projection and back ground scattering intensity, etc., it can be interpreted that the liquid-quenched alloy prepared at a fast quenching rate is almost isotropic and homogenious. Furthermore, it may be supposed that no preferred orientation is developed appreciably during liquid-quenching and also in crystallization process as well (as far as this pole figure determination is concerned).

Similar results were also obtained with the cold-rolled sheet of the liquid-quenched $Fe_{80}P_{13}C_7$ alloy prepared at a fast quenching rate. Figure 12(c) illustrates the pole figure obtained by using the reflection which produces the first halo ring of the cold-rolled sheet and Fig. 12(d) illustrates the pole figure obtained with the (110) reflection of αFe matrix in the sheet which was cold-rolled and crystallized at about 600°C. It may be assumed from these figures that there are no microcrystallites large enough to give a preferred orientation in the rolling texture or in the crystallized phase.

IDENTIFICATION OF AMORPHOUS ALLOYS

When an amorphous alloy is obtained by means of either the vapour-quenching , the electro- or electroless deposition, the liquid-quenching, etc., X-ray or electron diffraction method is usually used to confirm the amorphous state. Furthermore, X-ray or electron diffraction analssis, namely, the radial distribution analysis of diffraction halos, has been generally used to determine the atomic structure of the amorphous alloy.

However, the information obtained this radial distribution analysis is averaged over a large area and the local fluctuations in the amorphous structure may be difficult to be detected in principle. For instance, in the present studies, a periodical fringe-like contrast or a circular arrangement of image spots was observed in the regions where the electron diffraction patterns consisted of only halo rings.

Therefore, it may be supposed that the amorphous structure is not one type of atomic arrangement but there are some kinds of atomic arrangements, which depend on the method and condition of preparation or the condition of annealing, in the amorphous alloys. Furthermore, it may also be considered that to identify the atomic structure of a liquid-quenched amorphous alloy or to characterize the amorphous alloys, the directer method such as high resolution electron microscopy or field-ion microscopy must be used in combination with X-ray or electron or neutron diffraction method.

TENSILE PROPERTIES

Tensile properties of liquid-quenched $Fe_{80}P_{13}C_7$, $Fe_{78}P_{15}C_7$ and $Fe_{78}B_{12}Si_{10}$ alloys were studied at room temperature by using an Instron-type testing machine.

The load-elongation curves of the liquid-quenched alloys prepared at the faster quenching rate were not straight and the deviation from the linearity existed well below the fracture point, as illustrated in Fig. 13(a). As compared with this, in the case of the alloys prepared at the lower quenching rate, the load-elongation curves were almost straight and the deviation from the linearity was nearly zero, as illustrated in Fig. 13(b).

In case the liquid-quenched alloys prepared at the faster quenching

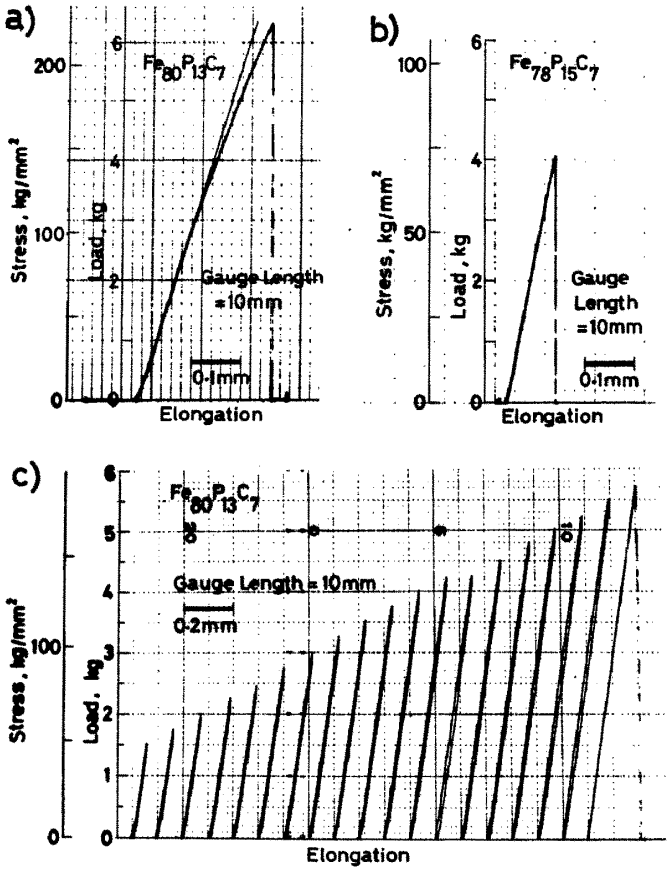

Figure 13. Load-elongation curves of liquid-quenched Fe-P-C alloys prepared at the faster quenching rate (a), and prepared at the slower quenching rate (b). Loading-unloading stress cycle made the load-elongation curve of the alloy prepared at the faster quenching rate to be almost straight (c).

rate were subjected to a series of loading-unloading stress cycles where the maximum load of each stressing cycle was gradually increased, the load-elongation curves became straighter and the deviation from the linearity of each curve was much smaller than the aforementioned case even at the fracture point, as illustrated in Fig. 13(c).

Figure 14(a) illustrates the scanning electron microscope (SEM) image of the liquid-quenched $Fe_{78}P_{15}C_7$ alloy which was prepared at the faster quenching rate and was fractured in tension at room temperature. The fracture modes consisted of three different ones which were similar to those observed by Pampillo et al. in the $Fe_{76}P_{16}C_4Al_3B_1$ amorphous alloy fractured in tension at room temperature [9]; a shear displacement (the smooth featureless region A), a pseudo-cleavage fracture (vein pattern B) and a mode similar to a very fine and shallow dimpled rupture C.

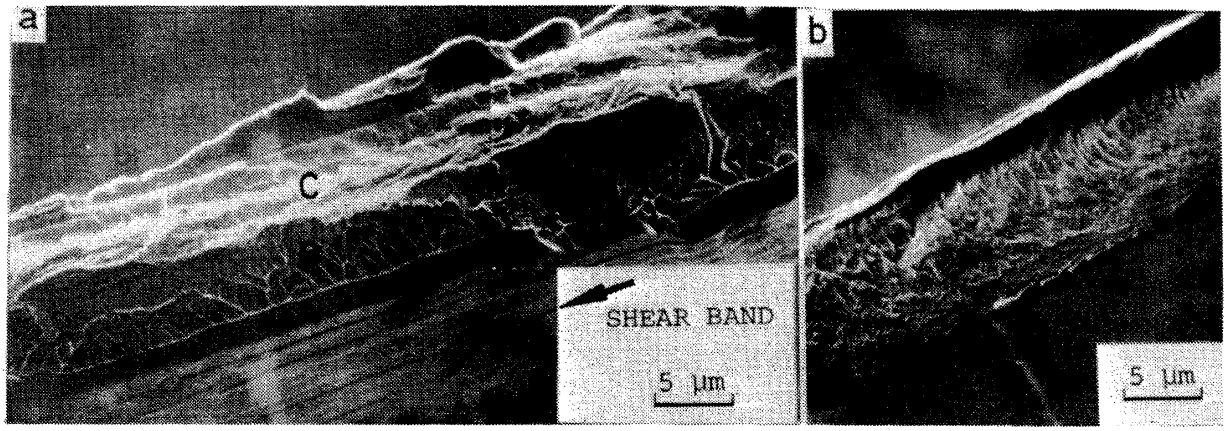

Figure 14. Tensile fracture surface of liquid-quenched $Fe_{78}P_{15}C_7$ alloy prepared at the faster quenching rate (a), and prepared at the slower quenching rate (b). Note that shear band like the one indicated by an arrow in (a) were not observed in (b).

Figure 14(b) illustrates the SEM image of the liquid-quenched $Fe_{78}P_{15}C_7$ alloy which was prepared at the slower quenching rate (hence a periodical fringe-like contrast was observed in this alloy) and was fractured in tension at room temperature. This fracture surface was quite similar to the fracture surface observed by Pampillo et al. in the $Ni_{37}Fe_{37}P_{14}B_6Al_3Si_3$ amorphous alloy failed at 190°K [10], that is, the occurrence of the shear displacement and hence the formation of the shear band did not occur and the fracture surface appeared flat with little or no traces of plastic flow. Judging from the load-elongation curve, the fracture mode and the untilted interference image, it may be assumed that existence of the domains where a periodical atomic arrangement existed probably embrittled these Fe-P-C and Fe-B-Si alloys prepared at the slower quenching rate.

REFERENCES

[1] W. Klement, Jr., R. H. Willens and P. Duwez: Nature, 187(1960) 869.
[2] H. Jones: Rep. Prog. Phys., 36(1973) 1425.
[3] S. Takayama: J. Mater. Sci., 11(1976) 164.
[4] B. C. Giessen and C. N. J. Wagner: Liquid Metals, ed. S. Beer (Marcel Dekker, New York) 1972, p. 633.
[5] G. S. Cargill III: Solid State Phys., 30(1975) 227.
[6] A. Howie, O. L. Krivanek and M. L. Rudee: Phil. Mag., 27(1973) 235.
[7] S. R. Herd and P. Chaudhari: phys. stat. sol. (a), 26(1974) 627.
[8] T. Masumoto, A. Inoue and H. Kimura: J. Japan Inst. Metals, 41(1977) 730 [in Japanese].
[9] C. A. Pampillo and D. E. Polk: Acta Met., 22(1974) 741.
[10] C. A. Pampillo: J. Mater. Sci., 10(1975) 1194.